

1 **SUPPLEMENTARY INFORMATION**

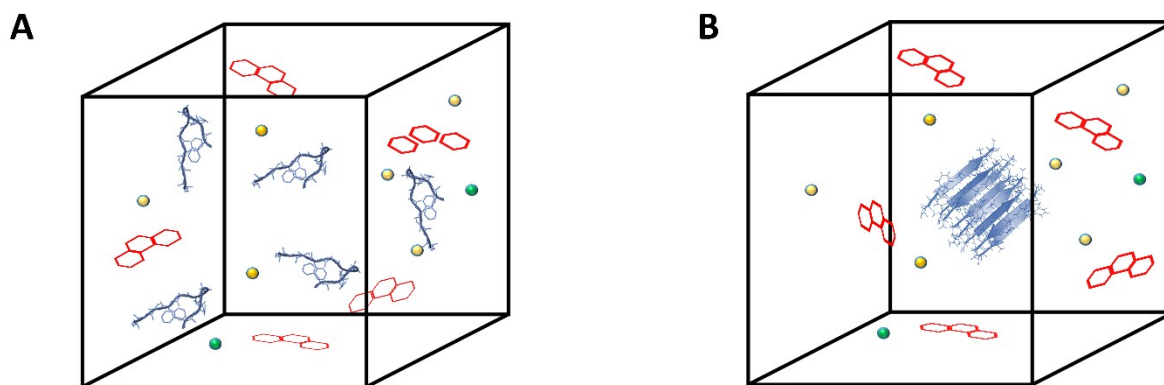
2 **DNA intercalators as amyloid assembly modulators: Mechanistic insights**

3 Jasdeep Singh, Ankit Srivastava, Pankaj Sharma, Prashant Pradhan, Bishwajit Kundu\*

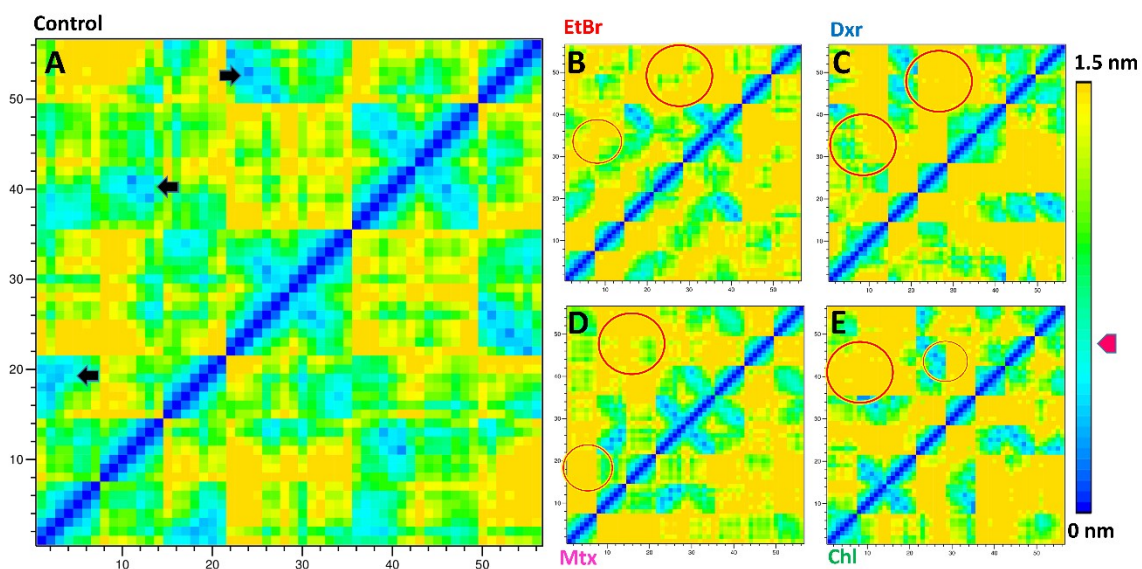
4 Kusuma School of Biological Sciences, Indian Institute of Technology Delhi, New Delhi, India

5

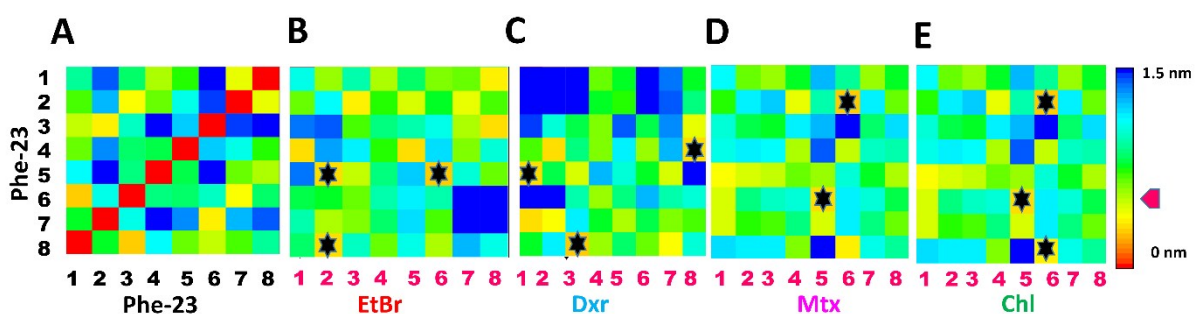
6



8 **Supplementary Figure 1:** Simulation boxes setup. (A) Cartoon representation for simulation of  
9 monomeric IAP (22-28)/AGel (186-192) peptides in the presence of intercalators. (B) Cartoon  
10 representation of simulation of IAP (22-28) protofibrillar assembly in the presence of intercalators.  
11 Counter ions are shown as solid spheres. Control systems represented unrestrained simulations of  
12 monomeric peptides and protofibril assembly alone.

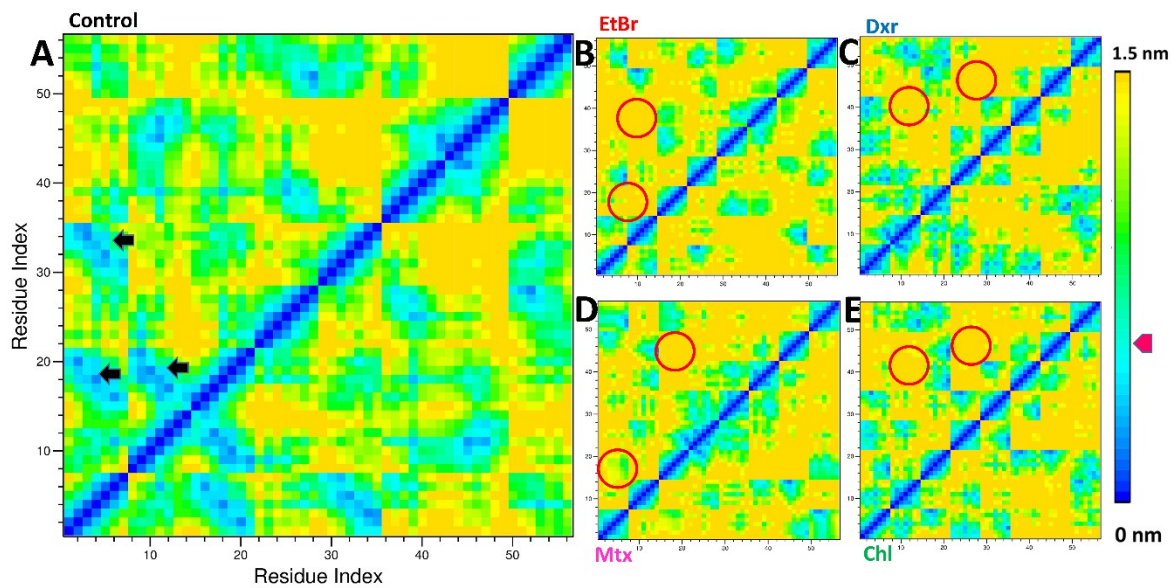


1  
 2 **Supplementary Figure 2:** MLDR of IAP (22-28) residues during its aggregation from monomers.  
 3 Representative MLDR's in the absence (A) and presence of EtBr, Dxr, Mtx and Chl (B-E). The  
 4 distance cut-off for major interactions (Pink arrow along scale bar) responsible for steering and  
 5 stabilization of assembly (Hydrogen bonds, Salt bridge, Pi-pi stacking) remains less than 5 Å. In  
 6 MLDR for control system (A), major areas showing gain in contacts as virtue of inter-residue distance  
 7 are shown arrow marked (Cyan to Blue regions). Integration of intercalators along monomeric units  
 8 resulted in increased inter-residue distance leading to loss contacts (circled red in B-E).



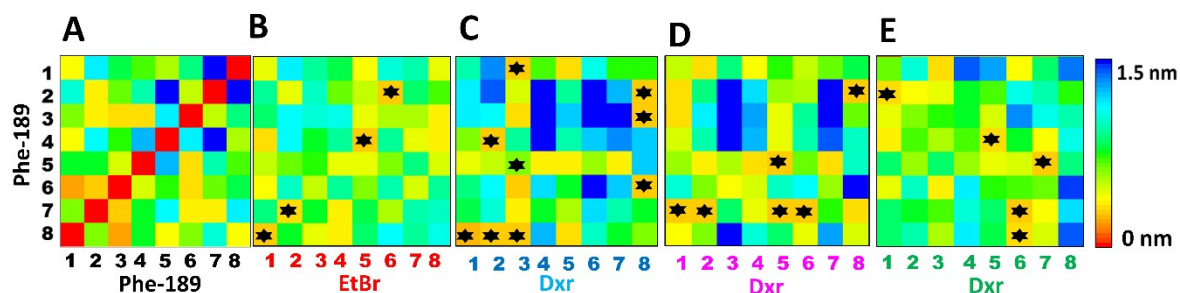
9  
 10  
 11 **Supplementary Figure 3:** MLDR representing associations of Phe-23 residues during IAP (22-28)  
 12 aggregation into octameric assembly. Aromatic/Hetero aromatic associations are defined considering  
 13 distance between the two ring centroids, less than 5 Å (face-to-face, pink marker along scale bar).  
 14 Inter molecular Phe-23 associations in control system averaged over last 400 ns are indicated through

1 cyan boxes (A). Loss of homomeric contacts in corresponding MLDR (Supplementary Figure 2) was  
 2 compensated through gain in heteromeric contacts (H-bonds and Aromatic associations) in the  
 3 presence of intercalators. (B-E) represents hetero-aromatic associations between Phe-23 from eight  
 4 monomeric chains (numbered black) and four different intercalators (EtBr, Dxr, Mtx and Chl  
 5 respectively, numbered pink). Dominant hetero-aromatic associations within the cut-off distance are  
 6 star marked.



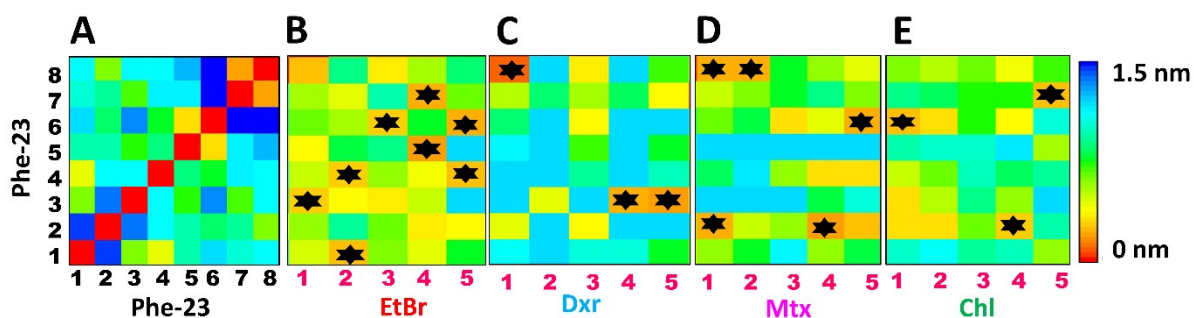
7  
 8 **Supplementary Figure 4:** MLDR of AGel (186-192) residues during its aggregation from  
 9 monomers. In MLDR for control system (A), major areas showing gain in contacts as virtue of inter-  
 10 residue distance are shown arrow marked (Cyan to Blue regions). Integration of intercalators along  
 11 monomeric units resulted in increased inter-residue distance leading to loss contacts (circled red in B-  
 12 E).

13  
 14



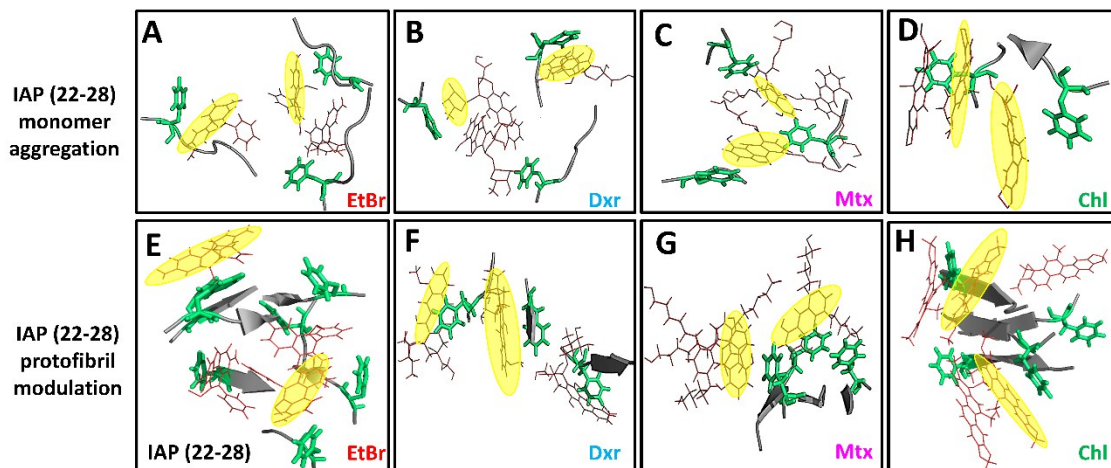
1

2 **Supplementary Figure 5:** MLDR representing associations of Phe-189 residues during AGel (186-  
 3 192) aggregation into octameric assembly. (A) indicates control systems showing inter molecular Phe-  
 4 189 associations in averaged over last 200 ns (Dark yellow boxes). (B-E) represents hetero-aromatic  
 5 associations between Phe-189 from eight monomeric chains (numbers colored as black) and different  
 6 intercalators (EtBr, Dxr, Mtx and Chl respectively, numbers colored as pink). Dominant hetero-  
 7 aromatic associations within the cut-off distance of 0.5 Å are star marked.



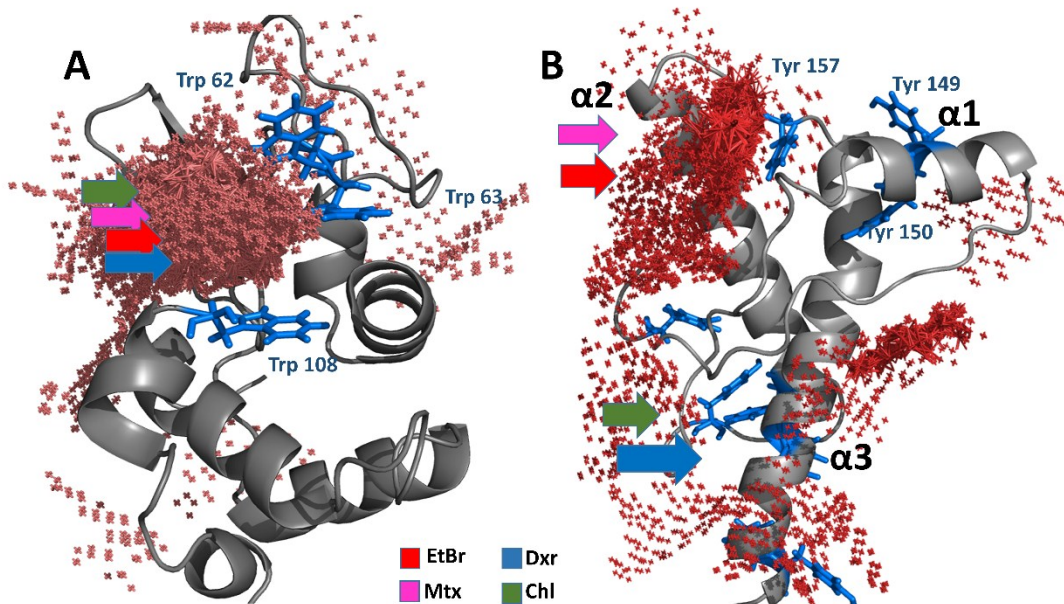
8

9 **Supplementary Figure 6:** MLDR representing associations of Phe-23 residues of pre-formed IAP  
 10 (22-28) octameric assembly with intercalators (A) Inter molecular Phe-23 associations in the absence  
 11 of intercalators averaged over last 400 ns. (B-E) represents hetero-aromatic associations between Phe-  
 12 23 from eight monomeric chains (numbers colored as black) and different intercalators (EtBr, Dxr,  
 13 Mtx and Chl respectively, numbers colored as pink). Numbered as 2, 4, 6 and 8 represent Phe-23  
 14 residues at fibril surface (Site 1) while 3 and 7 are confined mostly to Site 2. Dominant hetero-  
 15 aromatic associations within the cut-off distance of 0.5 Å are star marked. EtBr and Dxr  
 16 destabilization of assembly can be observed through hetero-associations with initially buried Phe-23  
 17 (3 and 7) residues of fibril core while Mtx and Chl associations are mostly mediated through Phe-23's  
 18 at surface.



1

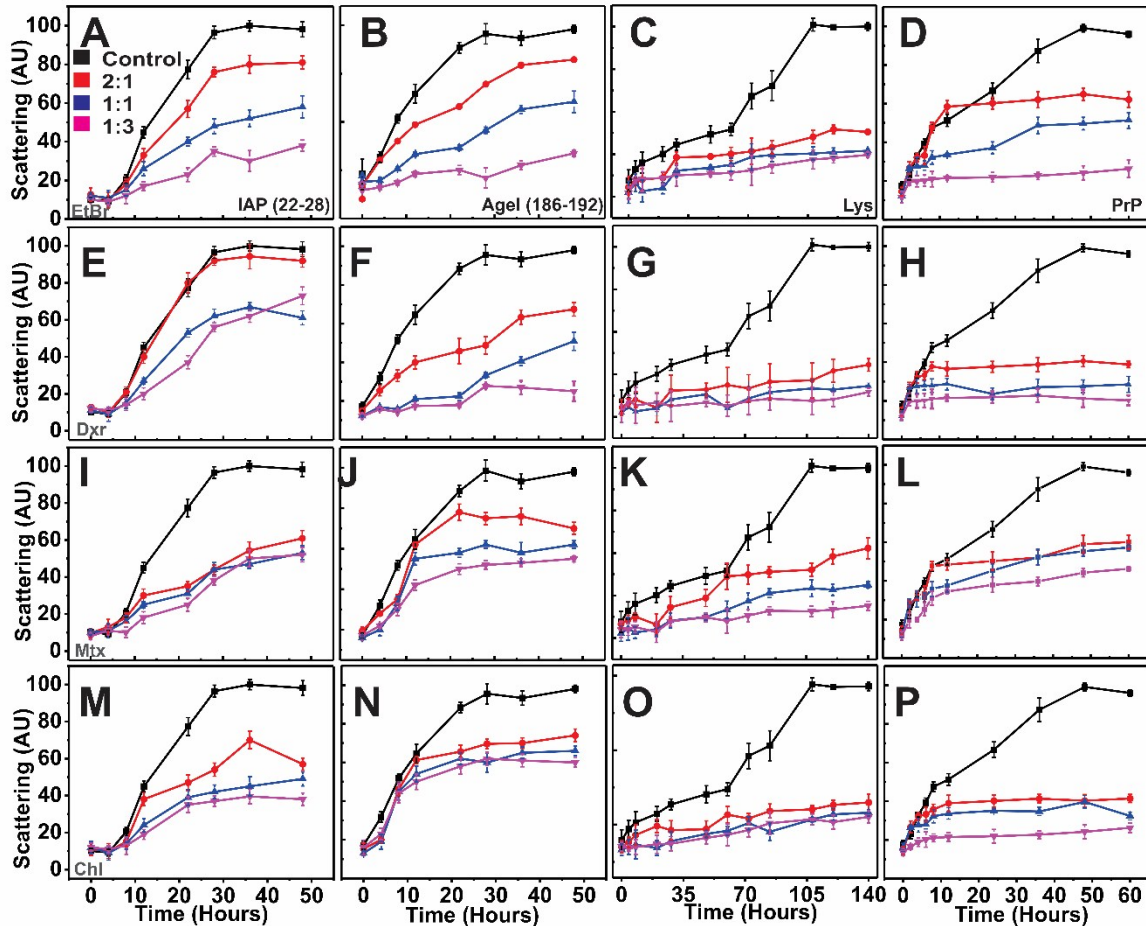
2 **Supplementary Figure 7:** Cartoon representation of hetero-aromatic associations. Phe-23 (colored  
 3 green) hetero-aromatic associations with the planar portion of intercalators (highlighted yellow; EtBr,  
 4 Dxr, Mtx and Chl respectively) during aggregation of IAP (22-28) monomers (A-D). Binding poses  
 5 for similar hetero-aromatic associations between Phe-23 of IAP (22-28) protofibril assembly and test  
 6 compounds (EtBr, Dxr, Mtx and Chl respectively) during assembly modulation (E-H). In all cases, the  
 7 distance between centroid of two planar rings for the given pose lies within cut-off limit ( $< 0.5 \text{ \AA}$ )  
 8 indicating aromatic associations.



9

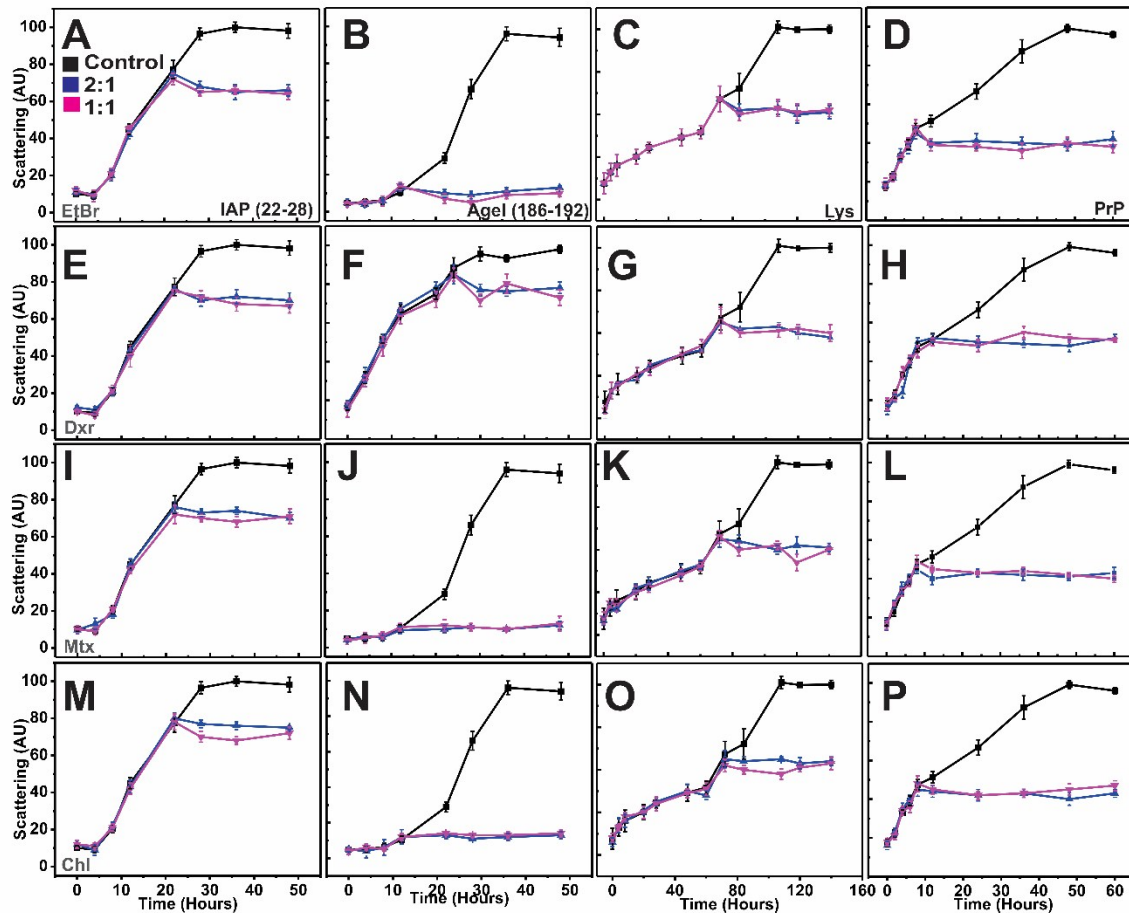
10 **Supplementary Figure 8:** Cluster analysis of binding poses of different intercalators with (A) Lys  
 11 and (B) PrP. (A) Preferred binding site (near the catalytic region involving residues, Glu 35, Asn 44,

1 Asn 46, Thr 47, Trp 62, Trp 63, Trp 108, and Val 109) of all four interactors are confined to original  
 2 Chl binding site. Highest binding energy poses (kcal/mol) were clustered to this site only (B) In PrP,  
 3 two preferred binding sites were observed, EtBr and Mtx at  $\alpha$ 2-helix while Dxr and Chl at  $\alpha$ 3-helix.



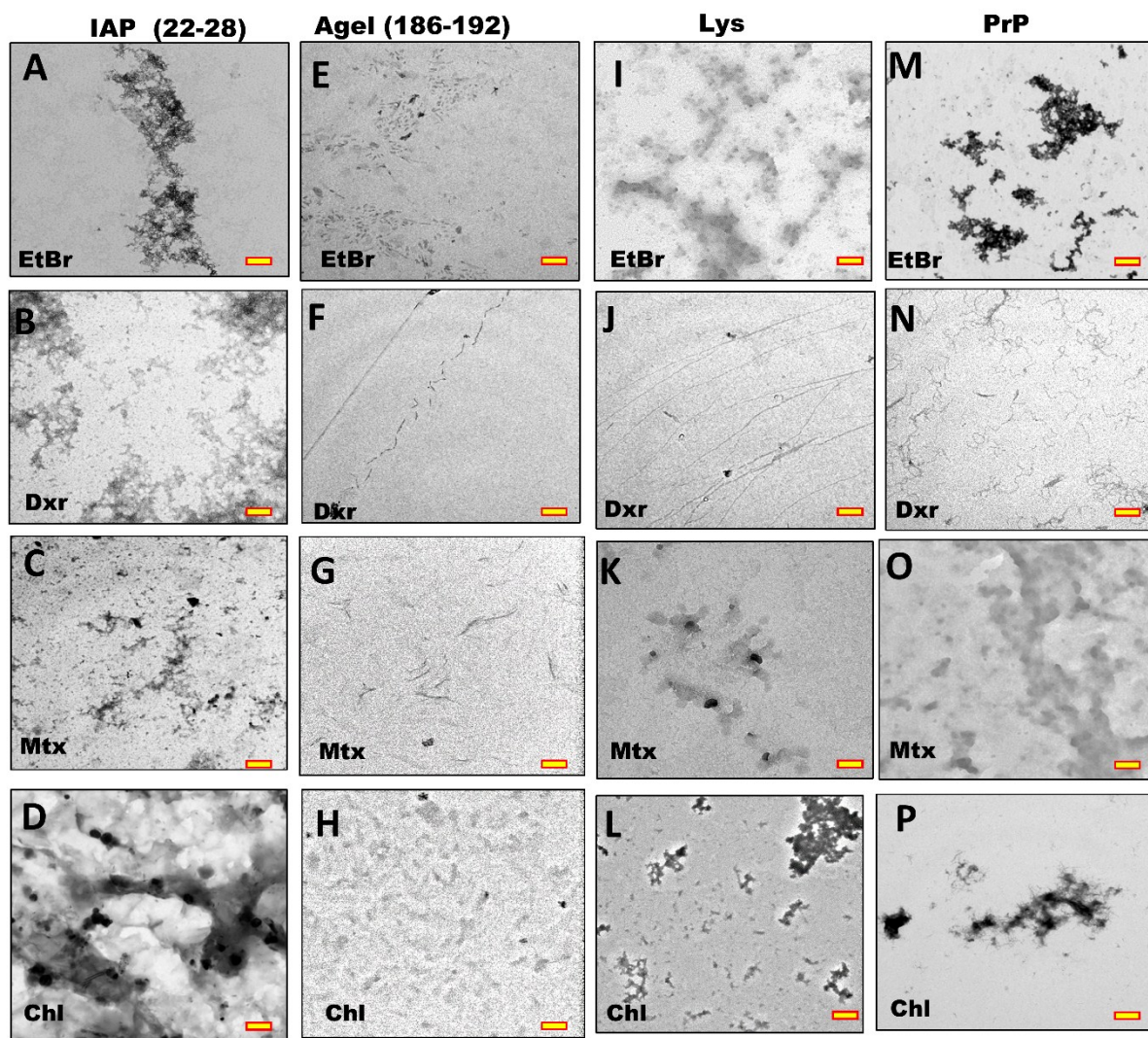
4

5 **Supplementary Figure 9:** Kinetics of scattering along the aggregation of peptide/protein monomers.  
 6 (A-D) Aggregation kinetics of IAP (22-28) (100  $\mu$ M), AGel (186-192) (100  $\mu$ M), Lys (140  $\mu$ M) and  
 7 PrP (30  $\mu$ M) in the absence (Black curves represents controls) and presence of EtBr at increasing P:D  
 8 molar ratios (Red 2:1, Blue 1:1 and Magenta 1:3) probed by monitoring light scattering ( $\lambda_{ex}$  and  $\lambda_{em}$  at  
 9 350 nm) when the compounds were pre-incubated at initiation of lag phases (0 hour). Similarly, (E-  
 10 H), (I-L) and (M-P) represents scattering kinetics in the presence of Dxr, Mtx and Chl respectively.  
 11 Error bars in each data point indicate standard deviation.



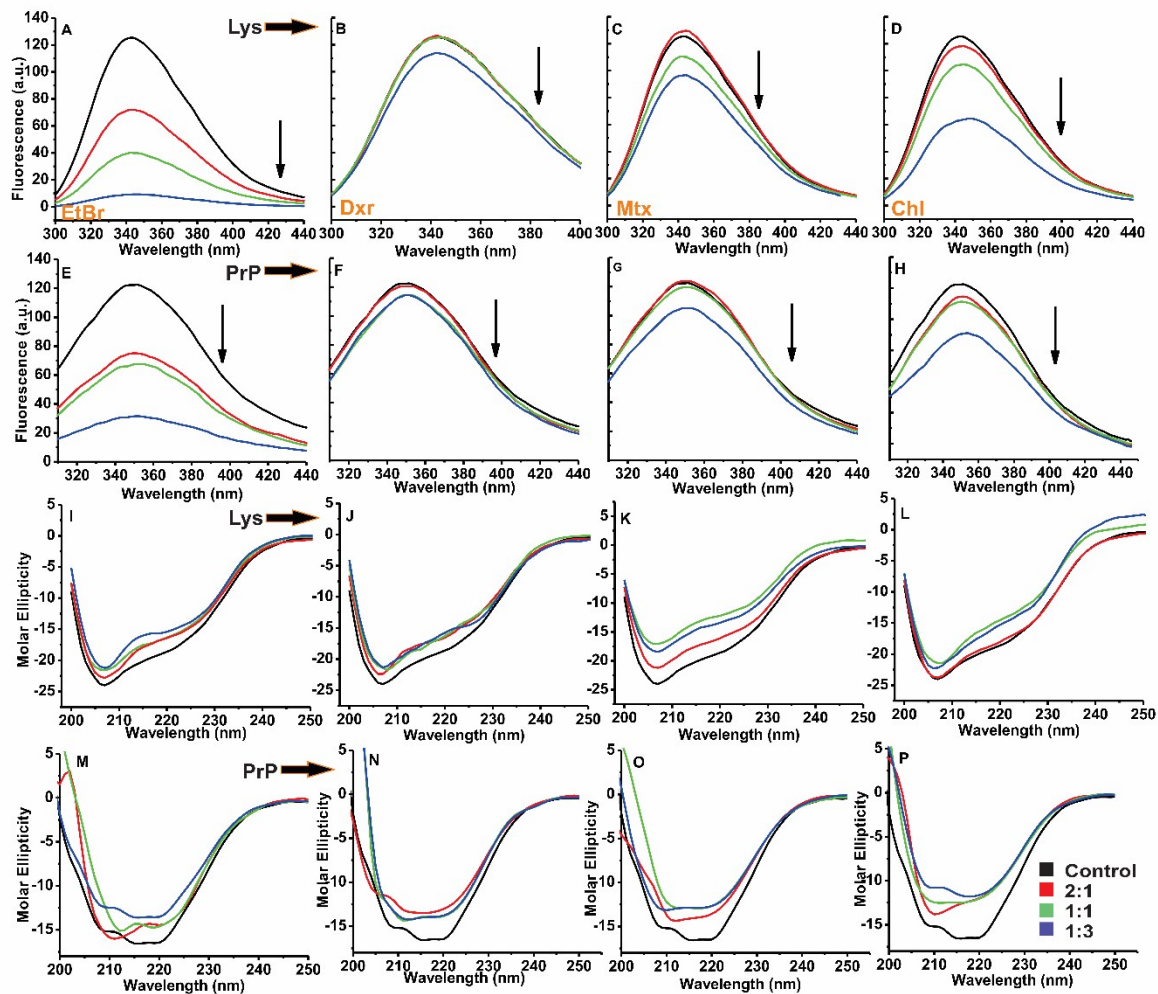
1

2 **Supplementary Figure 10:** Modulation of protofibril progression probed through SLS. (A-D)  
 3 Aggregation kinetics of IAP (22-28) (100  $\mu$ M), AGel (186-192) (100  $\mu$ M), Lys (140  $\mu$ M) and PrP (30  
 4  $\mu$ M) in the absence (Black curves represents controls) and presence of EtBr at increasing molar ratios  
 5 (Blue 2:1 and Magenta 1:1) probed by monitoring light scattering when the compounds were  
 6 incubated during exponential growth phase of each system. Similarly, (E-H), (I-L) and (M-P)  
 7 represents scattering kinetics in the presence of Dxr, Mtx and Chl respectively. Error bars in each data  
 8 point indicate standard deviation.



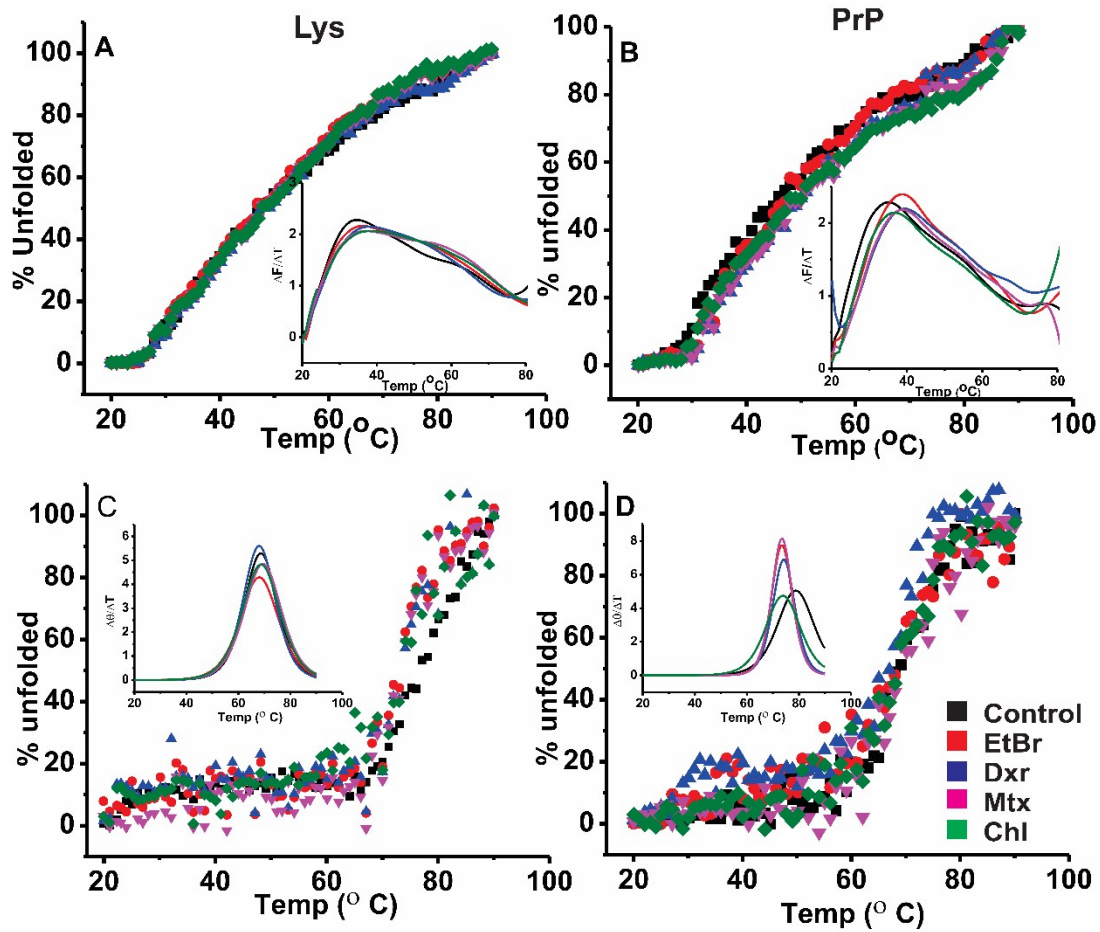
1

2 **Supplementary Figure 11:** TEM images of assembly formation after the compounds were added  
 3 during exponential growth phase (at 2:1 ratio corresponding to Figure 7). End stage aggregates of IAP  
 4 (22-28), AGel (186-192), Lys and PrP in the presence of EtBr. Corresponding systems in the  
 5 presence of Dxr, Mtx and Chl are shown in B-P. All intercalators restricted the pathways to growth-  
 6 incompetent protofibrillar states. Scale bars (yellow insets) are 500 nm.



1  
2

3 **Supplementary Figure 12:** Tertiary and secondary structure transitions induced by intercalators at  
 4 increasing concentrations. Lys and PrP (2  $\mu$ M) were pre-incubated with different intercalators at P:D  
 5 molar ratios of 2:1, 1:1 and 1:3 for 4 hours prior taking measurements. (A-D) and (I-L) represent  
 6 tertiary and secondary structure transitions in Lys respectively. (E-H) and (M-P) represent tertiary and  
 7 secondary structure transitions in PrP respectively. Identical buffer conditions in all cases were  
 8 employed for which respective aggregations were carried out.



1

2 **Supplementary Figure 13:** Assessment of structural stability conferred by intercalators to proteins,  
 3 Lys and PrP. Thermal melting of Lys and PrP probed by monitoring changes in  $\lambda_{340}$  (Tertiary  
 4 structure transitions, A and B) and  $\theta_{222}$  (Secondary structure transitions, C and D) with increase in  
 5 temperature for control system (Black) and in the presence of intercalators (Red: EtBr, Blue: Dxr,  
 6 Green: Mtx and Chl: Magenta). Normalized data is plotted as percent unfolding induced by  
 7 temperature increments. Insets represents first derivatives of melting curves where the maxima  
 8 indicates  $T_m$  (melting temperature) of the corresponding system. Identical buffer conditions in all  
 9 cases were employed for which respective aggregations were carried out.

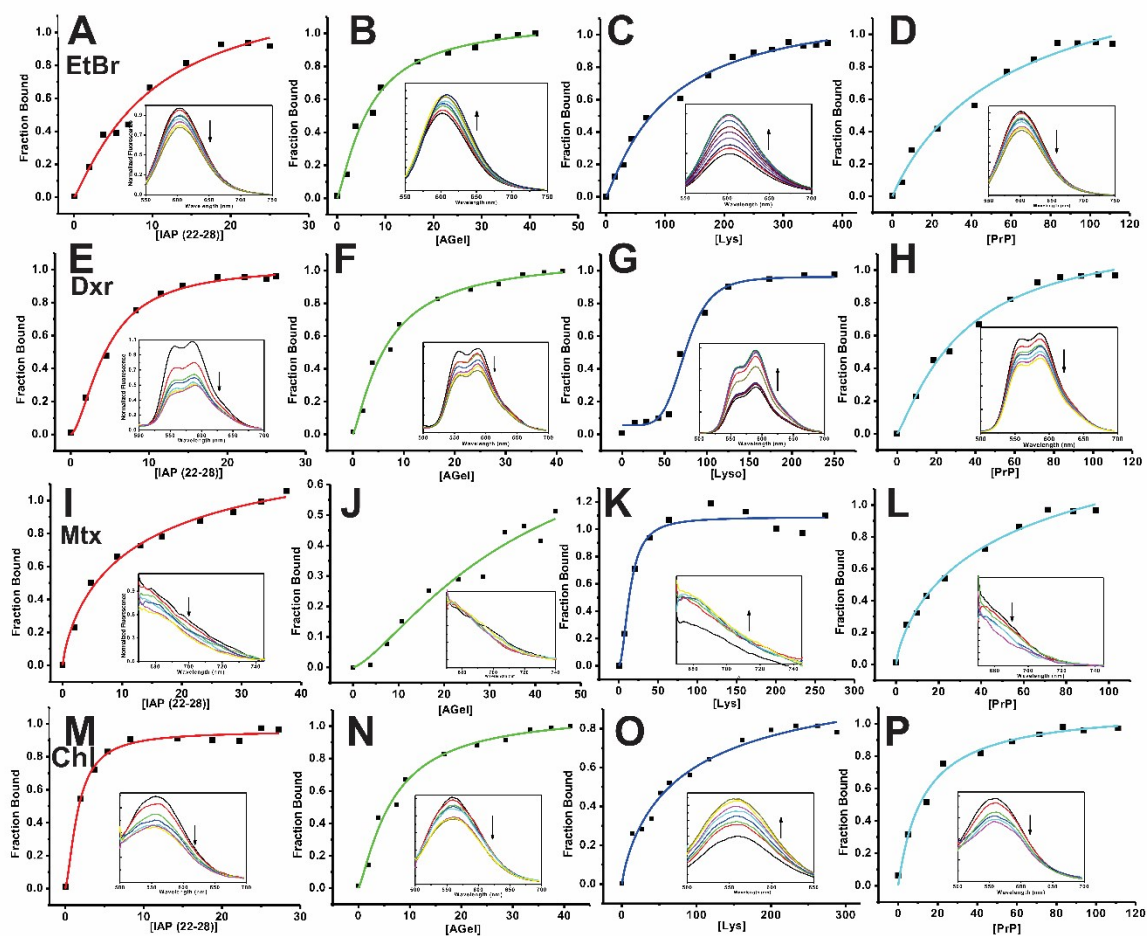
10

11

12

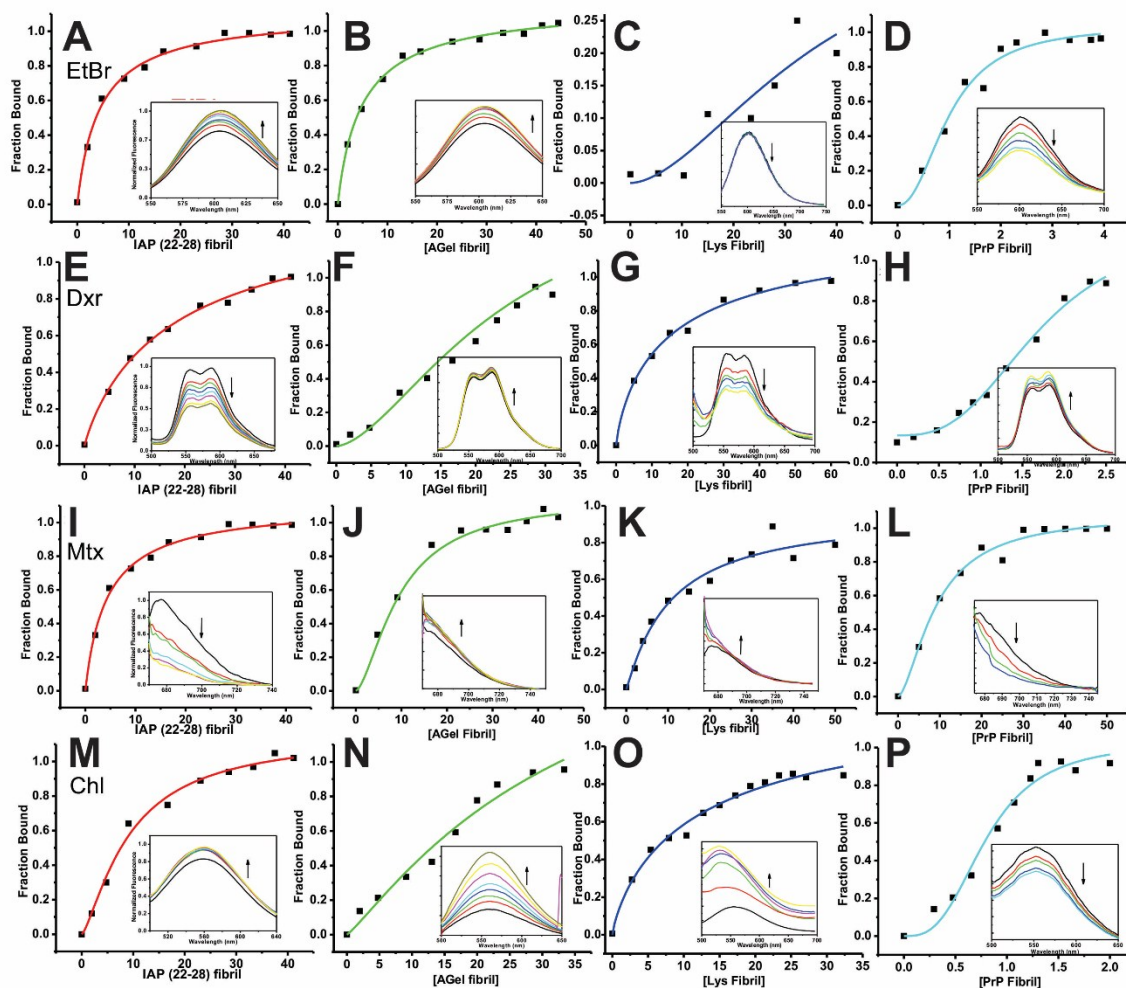
13

14



1  
 2 **Supplementary Figure 14:** Binding affinity studies of intercalators with monomeric  
 3 proteins/peptides. Single site non-linear curve fits for association of EtBr to IAP (22-28), AGel (186-  
 4 192), Lys and PrP monomers (A-E) are plotted as fraction bound vs total compound concentration (in  
 5  $\mu\text{M}$  for all cases). Drug concentration in each case was kept constant at  $2 \mu\text{M}$ . Insets show titration  
 6 curves depicting change in fluorescence emission of compound upon addition of peptide/protein  
 7 monomers. Similarly, (E-H), (I-L) and (M-P) represent datasets for Dxr, Mtx and Chl binding to  
 8 monomers. Binding of Mtx with AGel (186-192) monomers (J) could not be determined by titrations  
 9 as no shifts in drug intensity were observed upon addition of peptide. Identical buffer conditions in  
 10 all cases were employed for which respective aggregations were carried out.

11  
 12  
 13  
 14



1  
2 **Supplementary Figure 15:** Binding affinity studies of intercalators with proteins/peptides fibrils.  
3 Single site non-linear binding curve fits for association of EtBr to IAP (22-28), AGel (186-192), Lys  
4 and PrP fibrils (A-E) are plotted as fraction bound vs total compound concentration (in  $\mu\text{M}$  for all  
5 cases). Insets show titration curves depicting change in fluorescence emission of compound upon  
6 addition of peptide/protein fibrils. Drug concentration in each case was kept constant at  $2 \mu\text{M}$ .  
7 Similarly, (E-H), (I-L) and (M-P) represent datasets for Dxr, Mtx and Chl binding to fibrils. Binding  
8 of EtBr with Lys fibrils (C) could not be determined by titrations as no shift in fluorescence was  
9 observed upon addition of fibrils. Identical buffer conditions in all cases were employed for which  
10 respective aggregations were carried out.

11

12

1 **Supplementary Table 1:** Docking and experimental free energy of binding with IAPP (22-28)  
 2 assembly. Estimated Free energy of binding (kcal/mol) of intercalators with IAP (22-28) fibril (PDB  
 3 id: 2kib) through docking at both sites by using MOE v2010.12 are given in first two columns.  
 4 Experimental binding free energies of compound association with fibrils are derived from dissociation

<b>Compound</b>	<b>Site 1</b>	<b>Site 2</b>	<b>Experimental</b>
<b>EtBr</b>	<b>-6.68±0.25</b>	<b>-5.8±0.13</b>	<b>-6.83±0.17</b>
<b>Dxr</b>	<b>-6.82±0.28</b>	<b>-5.87±0.14</b>	<b>-6.44±0.32</b>
<b>Mtx</b>	<b>-6.59±0.15</b>	<b>-5.72±0.11</b>	<b>-6.42±0.28</b>
<b>Chl</b>	<b>-7.11±0.23</b>	<b>-5.74±0.18</b>	<b>-6.86±0.22</b>

5 constants determined through fluorescence titrations (Supplementary Table 5) by using equation:

6  $\Delta G^\circ = -RT \ln K_d$  at T = 298 K.

7

8 **Supplementary Table 2:** Best docking free energy of binding of intercalators with proteins.  
 9 Estimated Free energy of binding (kcal/mol) of intercalators with Lys and PrP through docking at  
 10 both sites by using MOE v2010.12 are given in first two columns.

<b>System</b>	<b>Lys</b>	<b>PrP</b>
<b>EtBr</b>	<b>-7.65±0.35</b>	<b>-6.69±0.2</b>
<b>Dxr</b>	<b>-7.43±0.49</b>	<b>-7.11±0.11</b>
<b>Mtx</b>	<b>-8.34±0.6</b>	<b>-7.18±0.21</b>
<b>Chl</b>	<b>-8.66±0.44</b>	<b>-8.44±0.28</b>

11

12 **Supplementary Table 3:** Lag phase duration (Hours, highlighted blue) and  $I_{max}$  (Maximum ThT  
 13 intensity, highlighted black) for aggregation kinetics of each system in the absence (Control) and  
 14 presence of different intercalators. Lag phase duration which could not be determined by fitting are  
 15 represented as NF.

System	IAP (22-28)	AGel (186-192)	Lys	PrP
<b>Control</b>	116.1±14.7	98.5±2.4	104.1±4.9	97.2±4.2
	19.1±2.4	25.1±0.7	75.7±5.4	6.3±0.5
<b>EtBr</b>	43.2±7.6	29.6±2.3	56.3±7.2	40.4±4.1
	14.8±2.7	25.8±2.2	41.8±1.1	37.2±4.5
<b>Dxr</b>	41.1±1.2	33.1±2.7	40.1±3.7	30.3±1.2
	7.7±3.1	26.3±1.4	NF	11.1±3.6
<b>Mtx</b>	58.7±19.0	28.5±1.5	46.1±1.6	66.8±3.8
	35.8±5.2	22.5±1.2	63.4±2.3	NF
<b>Chl</b>	45.9±3.5	24.1±1.1	40.6±2.1	64.5±2.1
	4.8±2.8	14.6±1.3	63.2±4.8	NF

1

2 **Supplementary Table 4:** Dissociation constants,  $K_d$  (in  $\mu\text{M}$ ) obtained from fluorescence titrations of  
3 intercalators with peptides/proteins monomers (Supplementary Figure 13). Single site fitting model  
4 was used to determine  $K_d$ . Dissociation constants which could not be determined by this protocol are  
5 represented as ND.

6

Compounds	IAP (22-28)	AGel (186-192)	Lys	PrP
<b>EtBr</b>	47±15	24.4±2.3	102±18	61.5±37.2
<b>Dxr</b>	23±1.3	6.65±1.1	74±3	33.5±6.55
<b>Mtx</b>	10±2.1	ND	14±1.8	62.5± 46
<b>Chl</b>	8.1±0.7	7±0.9	85±4.2	12.9±2.7

7

8

9 **Supplementary Table 5:** Dissociation constants,  $K_d$  (in  $\mu\text{M}$ ) obtained from fluorescence titrations of  
10 intercalators with peptides/proteins fibrils (Supplementary Figure 13). Single site fitting model was  
11 used to determine  $K_d$ . Dissociation constants which could not be determined by this protocol are  
12 represented as ND.

13

Compounds	IAP (22-28)	AGel (186-192)	Lys	PrP
<b>EtBr</b>	9.8±0.9	5.4±0.4	ND	61.5±37.2

<b>Dxr</b>	<b>19±6.2</b>	<b>23±15</b>	<b>16.4±6.7</b>	<b>33.5±6.55</b>
<b>Mtx</b>	<b>4.1±0.5</b>	<b>9.62±1.4</b>	<b>10.6±4.1</b>	<b>62.5± 46</b>
<b>Chl</b>	<b>9.29±1.5</b>	<b>35±4.1</b>	<b>13.3±7.4</b>	<b>12.9±2.7</b>

- 1
- 2
- 3
- 4